Photoacoustic frequency-domain depth profilometry of surface-layer inhomogeneities: Application to laser processed steels

Tian-Chi Ma,[a] Mahendra Munidasa, and Andreas Mandelis
Photothermal and Optoelectronic Diagnostics Laboratory, Department of Mechanical Engineering, University of Toronto, Toronto, Ontario, Canada M5S 1A4

(Received 16 December 1991; accepted for publication 11 March 1992)

An observed change in the photoacoustic signal frequency response of laser processed stainless-steel and carbon steel samples with respect to unprocessed reference samples is reported. A recently developed thermal wave theory for depth profiling of bulk inhomogeneities (where the surface thermal diffusivity is known and is the same as the homogeneous reference material) in condensed phases with arbitrary, continuously varying thermal diffusivity profiles [A. Mandelis, S. B. Peralta, and J. Thoen, J. Appl. Phys. **70**, 1761 (1991)] has been modified to obtain quantitative thermal diffusivity profiles extending from the surface into the bulk. Profiles obtained using this method, which is, in principle, of nondestructive nature, are consistent with the profiles obtained from destructive methods such as cross-sectional optical metallographic examination and microhardness testing.

I. INTRODUCTION

Photoacoustic and photothermal detection methods have evolved rapidly as a very effective way of nondestructive testing complimentary to conventional methods such as ultrasound and x-ray inspection. These methods have advantages especially for near-surface detection with a variable depth range, compared to conventional techniques. In this family of methods a beam of energy (laser or electron beam), modulated at a certain frequency is focused onto the sample surface. The resulting periodic heat flow in the material is a diffusive process, producing a periodic temperature distribution which is called a "thermal wave." These waves will reflect and scatter from features beneath the surface which have different thermal characteristics from their surroundings. Thermal waves are heavily damped, their amplitude decreasing by a factor of e^{-1} within a distance from the surface of one thermal diffusion length. The thermal diffusion length (penetration depth) μ is given by

$$\mu = \sqrt{\frac{\alpha}{\pi f}}, \tag{1}$$

where α is the thermal diffusivity of the medium and f is the modulation frequency. Several different detection methods[1,2] have been used to detect these thermal waves.

Reconstruction of the thermal diffusivity profiles of inhomogeneous solids from the frequency-domain surface data is a very important manifestation of the nondestructive evaluation capabilities of the photoacoustic technique. Such a reconstruction method based on the Hamilton–Jacobi formulation of thermal-wave physics[3] has recently been reported.[4] This method has been used to reconstruct thermal diffusivity profiles 20–30 μm below the surface[5] of liquid crystal samples upon application of a transverse magnetic field. In those samples, the surface diffusivity α_0 was unchanged and was the same as the thermally homogeneous reference sample (the same liquid crystal without the magnetic field). However, many applications such as surface-treated materials, radiation damage in solids, etc., are found where the inhomogeneity exists in the surface layer. The bulk in these samples is unchanged and is the same as the reference. In this paper we extend the formulation and reconstruction algorithm described in Refs. 4 and 5 in profiling surface layer (rather than bulk) inhomogeneities. Then we apply this method to obtain quantitative thermal diffusivity profiles of laser processed stainless steel and low carbon steel.

Surface engineering with laser can be divided into the following categories:[6] laser transformation hardening (LTH); laser surface melting (LSM); laser surface alloying (LSA); and laser surface cladding (LSC). The low power density processes of transformation hardening rely on surface heating without melting. Processes which rely on surface melting require higher power densities to overcome the conduction heat losses; such processes include simple surface melting to achieve greater homogenization. The melting processes also include those where a material is added either with a view to mixing into the melt pool as in surface alloying or with a view to fusing on a thin surface melt as in cladding. All the above-mentioned processes are either in production or are being very seriously considered for production. The common advantages of laser surfacing compare to alternative processes are chemical cleanliness, controlled thermal penetration and therefore distortion, controlled thermal profile and therefore shape and location of the thermally affected region, and noncontact processing. In selecting and controlling the laser processing parameters to optimize surface improvement, it is very important to evaluate the effects caused by laser processing. The fundamental problem here is to profile the processed layer. Other photothermal methods have previously been applied to study surface hardening of steel.[7,8] Advantages of our method over those techniques are described elsewhere.[4]

[a]On leave from Quantum-Electronics Institute, South China Normal University, Guangzhou, China.

 0021-8979/92/126029-07$04.00

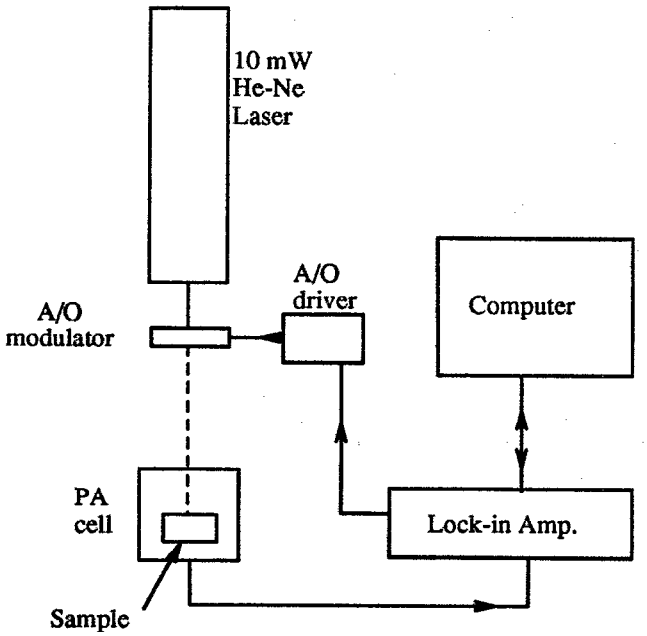

FIG. 1. Schematic diagram of the experimental setup.

In this work we performed detailed studies of the frequency dependence of the photothermal signal from laser processed and regular stainless-steel and low carbon steel samples using the photoacoustic (PA) gas-cell detection method. Then we solved the inverse problem to extract quantitative depth profiles of the thermal diffusivity.

II. EXPERIMENTAL AND SAMPLE PREPARATION

A schematic diagram of the experimental apparatus is shown in Fig. 1. The sample is mounted inside an airtight cell supplied with a remote, sensitive microphone. A 10 mW He–Ne laser modulated by an acousto-optic (A/O) modulator is directed onto the sample surface through an optical window in the cell. The laser beam spot size on the sample surface is about 1.5 mm. Periodic pressure variations (photoacoustic signal) in the cell due to the periodic heating of the sample are detected by the microphone mounted inside the cell. The microphone signal proportional to the periodic temperature profile of the sample surface,[9] integrated over the beam spot size, is detected via a lock-in amplifier (EG&G model 5210). The lock-in amplifier internal oscillator is used to modulate the laser beam. In this work we used a commercial photoacoustic sample cell assembly with a builtin preamplifier (EG&G model 6003) and its power supply (model 6005). The lock-in is interfaced with a personal computer so that the frequency scan and the data acquisition and storage are automated.

Several samples of low carbon steel (0.042% C) and stainless steel (type 301) were laser processed at various beam spot diameters and scanning speeds. The processing was performed with a 1.5 kW CO_2 laser with 1 kW cw output at speeds varying from 1 to 2 in./s, and at beam spot diameters from 0.3 to 0.9 mm. In order to achieve wide enough laser processed area, some overlapping was allowed between laser scans. Detailed study of one sample from each steel type is presented here.

Samples were machined to the shape of the sample holder inside the cell, from the original laser processed specimens. Reference samples were machined from unprocessed original material. For each sample surface, the PA signal amplitude and phase were recorded in the modulation frequency range between 10 and 500 Hz. The frequency increment was 2 Hz. The lower frequency limit was dictated by the requirement that the air column above the sample be thermally thick. This avoids any signal behavior complications due to propagation of heat through the walls of the cell.[9] The upper limit was determined by the signal-to-noise ratio and complications due to cavity resonances in the cell-microphone assembly. For each surface, data were averaged over three to five experimental runs to reduce random noise.

In order to compare PA measurement results with the microstructure of the surface layers of laser processed samples, specimen cross sections were characterized by optical microscopy. After the PA experiments the samples were cut normal to the laser processed direction for metallographic examinations. Hardened zones were determined by normal etching techniques and by microhardness testing, using a Vickers indenter with 100 g load. The hardened zones obtained with all tests were of lenticular shape that is found when processed with a defocused low order mode laser beam. From the metallographic photographs (optical) and microhardness profile, the depths of hardened zones were measured.

III. RESULTS

A. Frequency response data

For each laser processed sample and its reference, the PA amplitudes were ratioed and the phases were subtracted, respectively. Variations in this amplitude ratio and the phase difference with frequency are related to the changes in the thermal diffusivity with depth due to processing. Before reconstructing the diffusivity profiles, smoothed frequency responses were obtained from the raw PA data using the earlier averaging techniques.[5] This helps to reduce the effect of random errors and improve the signal-to-noise ratio. Further discussion of this smoothing technique, its importance, and the effect of data smoothing on reconstructed profiles can be found in Ref. 5.

Plots in Figs. 2(a) and 2(b) show the subtracted phase data before and after smoothing from a low carbon steel [Fig. 2(a)] and a stainless-steel [Fig. 2(b)] sample. Processing parameters for the carbon steel sample are 1 in./s scan speed and 0.9 mm spot size, and for the stainless-steel sample laser scan speed was 1 in./s and the spot size 0.3 mm. The laser processed surface has been compared with the unprocessed reference, of the same material. Figures 2(c) and 2(d) show the corresponding amplitude ratios. These data clearly show the difference in the signal due to laser processing.

Polished and etched cross sections of the laser pro-

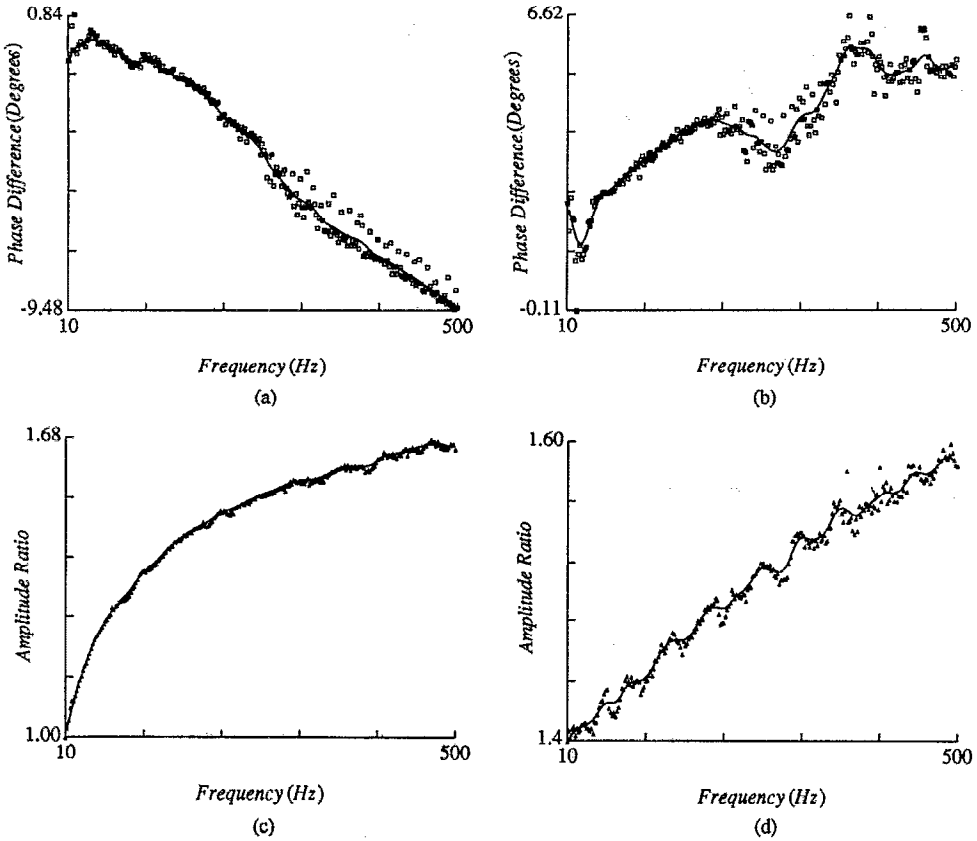

FIG. 2. PA signal phase difference between (a) the low carbon steel laser processed surface; (b) the stainless-steel laser processed surface, and the corresponding unprocessed reference vs frequency. PA signal amplitude ratio between (c) the low carbon steel laser processed surface; (d) the stainless-steel laser processd surface, and the corresponding unprocessed reference vs frequency. Solid lines represent data after smoothing.

cessed low carbon steel and the stainless-steel sample when observed under an optical microscope are shown in Fig. 3. Microhardness profiles obtained from the Vickers microhardness test on cross sections of both samples are shown in Fig. 4. The photograph 3(a) of the stainless-steel sample cross section clearly shows two main features due to typical solidification produced by complete melting and resolidification: (1) fine equiaxied crystals on the top layer due to very fast cooling rate; (2) a second layer, dendritic morphology, aligned in the direction of the heat flow, normal to the surface. A sharp boundary between the laser heat affected zone and the bulk of the material can be clearly seen. The microhardness test shows an increase in hardness towards the surface from a depth of approximately 200 μm [Fig. 4(a)]. The cross sectional photograph [Fig. 3(b)], of the low carbon steel sample shows the ferrite crystals in the surface layer have become smaller after laser treatment but the boundary is not very clear, and no dendritic morphology can be seen. The microhardness test shows an increase in hardness towards the surface from a depth of approximately 120 μm [Fig. 4(b)]. The microhardness profiles of the samples indicate that there is some increase in microhardness in the surface layer after laser processing for both materials. This trend is more significant for the stainless steel. It is assumed that for the low carbon steel sample when the laser is scanned across the surface, the ferrite phase transformed to austenitic phase. During rapid cooling after the laser beam advanced, the austenite phase transformed to ferrite but the crystals became smaller due to inadequate growth time. Since the carbon content was very low in the material, no martensitic transformation was assumed to have occurred during cooling.

B. Theoretical: Reconstruction of thermal diffusivity profiles from data

The frequency-dependent surface temperature $T(\omega)$ of an inhomogeneous optically opaque sample is given by[4]

$$T(\omega)=T_0(\omega)\left\{1-\tfrac{1}{4}R^{1/2}(\infty)\times\exp\left[-\frac{(1+i)\sqrt{\omega}}{2\sqrt{2q}}\frac{1}{\sqrt{\alpha_\infty}}\ln\left(\frac{\alpha_\infty}{\alpha_0}\right)\right]\right\}, \tag{2}$$

where a monotonically increasing thermal diffusivity depth profile ($\alpha_\infty>\alpha_0$) of the form

$$\alpha_s(x)=\alpha_0\left(\frac{1-\Delta e^{-qx}}{1-\Delta}\right)^2, \quad \text{where } \Delta\equiv 1-\left(\frac{\alpha_0}{\alpha_\infty}\right)^{1/2} \tag{3}$$

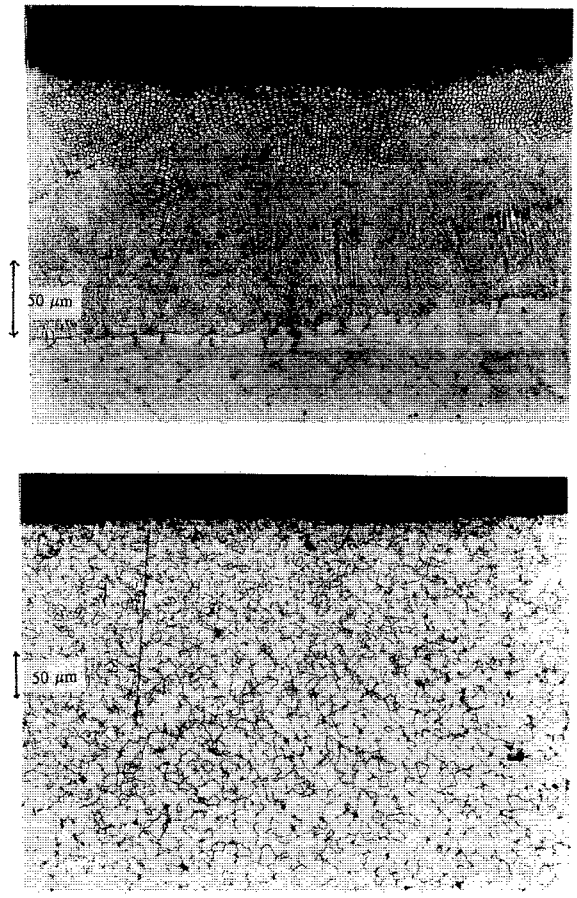

FIG. 3. Optical microscope photograph of the cross section of the laser processed layer in (a) the stainless steel, and (b) the low carbon steel sample.

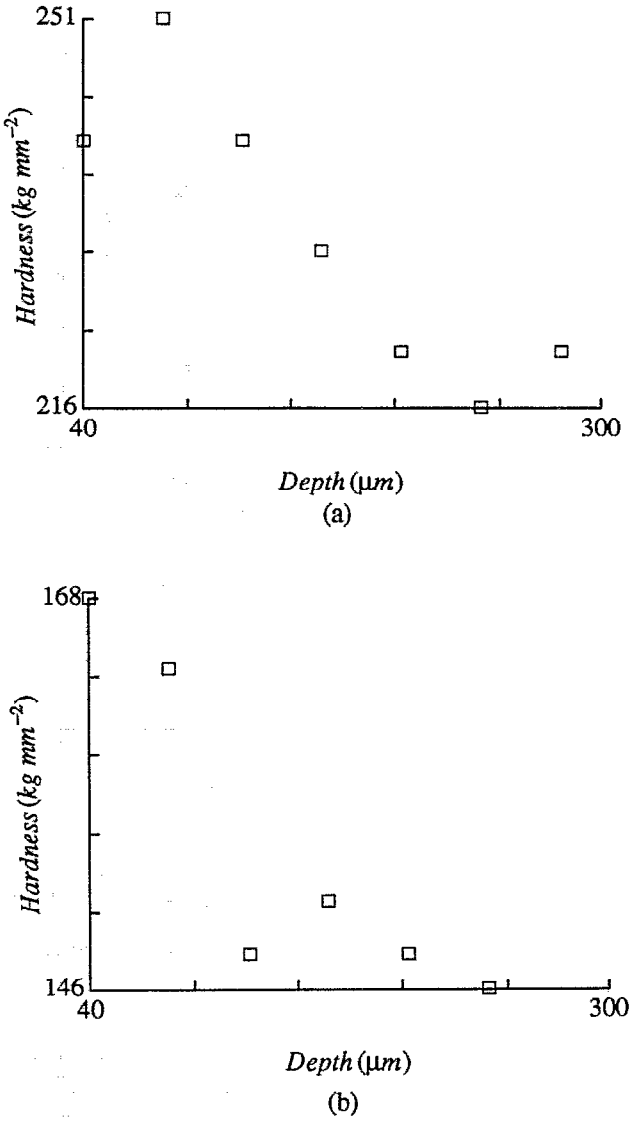

FIG. 4. Hardness obtained from the Vickers hardness test vs depth from laser processed (a) stainless steel, and (b) low carbon steel.

is assumed. Here α_0 and α_∞ are thermal diffusivities at the surface ($x=0$) and the bulk, respectively, and q determines the rate of change of $\alpha_s(x)$. In Eq. (2)

$$R(x)\equiv e_s(0)/e_s(x), \tag{4}$$

where $e_s(x)$ is the depth-dependent thermal effusivity; $e_s(x)=[k(x)\rho(x)c(x)]^{1/2}$, with k, ρ, c, respectively, the thermal conductivity, density, and specific heat, of the sample. The surface temperature of a condensed medium with homogeneous diffusivity α_j due to an incident flux Q_0 is given by[3,4]

$$T_j(\omega;\alpha_j)=\frac{Q_0}{k_j\sigma_j};\quad j=0 \quad \text{or} \quad \infty, \tag{5}$$

where $\sigma_j=(1+i)(\omega/2\alpha_j)^{1/2}$.

The frequency response signal of a continuously thermally inhomogeneous solid sample when normalized by the response of a homogeneous reference sample (with thermal diffusivity α_∞) of surface temperature $T_0(\omega)$, is given upon division of Eq. (2) by Eq. (5) with $j=\infty$:

$$|M(\omega)|e^{i\Delta\phi(\omega)}=\frac{1}{R(\infty)}\left\{1-\frac{1}{4}R^{1/2}(\infty)\times\exp\left[-\frac{(1+i)\sqrt{\omega}}{2\sqrt{2q}}\frac{1}{\sqrt{\alpha_\infty}}\ln\left(\frac{\alpha_\infty}{\alpha_0}\right)\right]\right\}, \tag{6}$$

where $|M(\omega)|$ is the amplitude ratio and $\Delta\phi(\omega)$ is the phase difference between the two samples. Separating Eq. (6) into real and imaginary parts leads to the following exact expressions for the thermal-wave amplitude ratio and phase difference:

$$|M(\omega)|^2=\frac{1}{R^2(\infty)}(1-\tfrac{1}{2}R^{1/2}(\infty)e^{-c\sqrt{\omega}}\times\cos(c\sqrt{\omega})+\tfrac{1}{16}R(\infty)e^{-2c\sqrt{\omega}}) \tag{7a}$$

and

$$\Delta\phi(\omega)=\tan^{-1}\left(\frac{\frac{1}{4}R^{1/2}(\infty)e^{-c\sqrt{\omega}}\sin(c\sqrt{\omega})}{1-\frac{1}{4}R^{1/2}(\infty)e^{-c\sqrt{\omega}}\cos(c\sqrt{\omega})}\right), \tag{7b}$$

where

$$c\equiv\frac{1}{2q}\left(\frac{1}{2\alpha_\infty}\right)^{1/2}\ln\left(\frac{\alpha_\infty}{\alpha_0}\right). \tag{8}$$

Although these expressions are valid for a monotonically increasing thermal diffusivity depth profile given by Eq. (3), arbitrary $\alpha_s(x)$ profiles can be handled by redefining (updating) the two constants (α_0,q) at every modulation frequency $f_j=\omega_j/2\pi$, starting with the highest frequency, from the experimental data values and assuming knowledge of the value of thermal diffusivity α_∞ of the homogeneous reference sample. Using the experimentally obtained values $|M(\omega)|$ and $\Delta\phi(\omega)$ at each frequency f_j, Eqs. (7a) and (7b) can be solved numerically to determine c_j and $R(\infty)_j$, i.e., the local values of c and $R(\infty)$. Assuming the effusivity ratio at $x=0$ and $x=\infty$ is adequately represented by the respective conductivity ratio, Eq. (4) leads to

$$\alpha_0\simeq\alpha_\infty R^2(\infty). \tag{9}$$

This approximation is valid, as it is known[7] that the changes in specific heat and density due to surface hardening of steel caused by other methods are much less pronounced than in thermal conductivity. This relationship is then used to calculate the local diffusivity $(\alpha_0)_j$ given by

$$(\alpha_0)_j\simeq\alpha_\infty R^2(\infty)_j. \tag{10}$$

Once $(\alpha_0)_j$ is calculated,

$$q_j=\frac{1}{2\sqrt{2}c_j\sqrt{\alpha_\infty}}\ln\left(\frac{\alpha_\infty}{(\alpha_0)_j}\right). \tag{11}$$

Now, numerically evaluated c_j can be used to evaluate locally at $\omega=\omega_j$ the q_j value. Then the thermal diffusivity profile $\alpha_s(x_j)$

$$\alpha_s(x_j)=(\alpha_0)_j\left(\frac{1-\Delta_j e^{-q_j\mu_{j-1}}}{1-\Delta_j}\right)^2,$$

where

$$\Delta_j\equiv1-\left(\frac{(\alpha_0)_j}{\alpha_\infty}\right)^{1/2} \tag{12}$$

can be found from Eq. (3). The calculation of the depth x_j is based on the fact that as modulation frequency decreases, the thermal-wave probing depth (thermal diffusion length) $\mu_j=\mu(\omega_j)$, Eq. (1) increases. Starting from the highest practical frequency ω_1, i.e., the shortest $x_1\sim\mu_1$, we can write

$$x_1=\mu_1\equiv\Delta\mu_1=[2(\alpha_0)_1/\omega_1]^{1/2}, \tag{13}$$

where we approximate a surface slice with $\alpha_s(x)\approx(\alpha_0)_1$. With decreasing frequency $f_j<f_{j-1}$, an increase in depth is given by

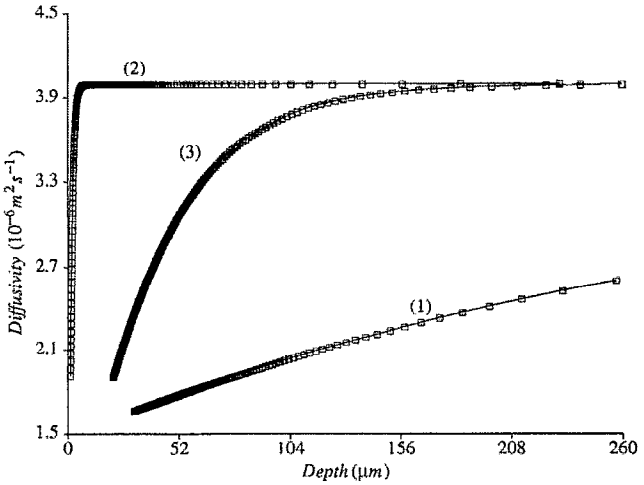

FIG. 5. Known thermal diffusivity profiles (solid line) using Eq. (3) and their discrete point reconstructions with (1) $q=3\times10^3$ m^{-1} and $\alpha_0=1.5\times10^{-6}$ m^2/s (10 to 500 Hz); (2) $q=1\times10^6$ m^{-1} and $\alpha_0=1\times10^{-8}$ m^2/s (20 Hz to 2.5 kHz); (3) $q=3\times10^4$ m^{-1} and $\alpha_0=7\times10^{-7}$ m^2/s (15 to 500 Hz). In each case $\alpha_\infty=4\times10^{-6}$ m^2/s.

$$\mu_j=\mu_{j-1}+\sqrt{\frac{2\alpha_j}{\omega_j}}-\sqrt{\frac{2\alpha_j}{\omega_{j-1}}}. \tag{14}$$

It is not possible to solve Eqs. (7a) and (7b) analytically for $R(\infty)_j$ and c_j. Equation (7b) can be solved for $R^{1/2}(\infty)_j$ in terms of c_j. Then substituting this in Eq. (7a) one equation results with c_j as the unknown parameter. Then, this equation is solved numerically based on Newton's method[10] for c_j and Eq. (7b) is used to calculate $R^{1/2}(\infty)_j$. To start the numerical search it is necessary to give an initial value to each c_j. For the first data point (highest frequency) an approximate value for c_1 was found based on the approximation $\delta f/f\ll1$ and $R(\infty)=1$, assuming local diffusivity $(\alpha_0)_1=\alpha_\infty$, [Eq. (6a) in Ref. 5]:

$$c_1=\left(\frac{2\sqrt{\omega_1}}{\delta\omega}\right)\ln\left(\frac{S(\omega_2)}{S(\omega_1)}\right), \tag{15}$$

where δf is the frequency increment and [Eq. (7) in Ref. 5]

$$S^2(\omega_1)\equiv|M(\omega_1)|^2+1-2|M(\omega_1)|\cos[\Delta\phi(\omega_1)]. \tag{16}$$

For the subsequent frequencies, the numerically obtained value of c_j from the previous frequency is used as the initial seed value.

In the following simulations we test the fidelity of the reconstruction of a known $\alpha_s(x)$ depth profile [from Eq. (3)] using the above procedure. Figure 5 shows three known profiles and corresponding reconstructions. Here, two extreme and one intermediate cases were chosen: (1) a slowly varying profile where $q=3\times10^3$ m^{-1} and $\alpha_0=1.5\times10^{-6}$ m^2/s (10 to 500 Hz); (2) a profile with a sharp drop near the surface nearly simulating an inhomogeneous thin layer on top of a homogeneous substrate, where $q=1\times10^6$ m^{-1} and $\alpha_0=1\times10^{-8}$ m^2/s (20 Hz to 2.5 kHz); and finally, an intermediate case (3) where $q=3\times10^4$ m^{-1} and $\alpha_0=7\times10^{-7}$ m^2/s (15 to 500 Hz). In each case α_∞

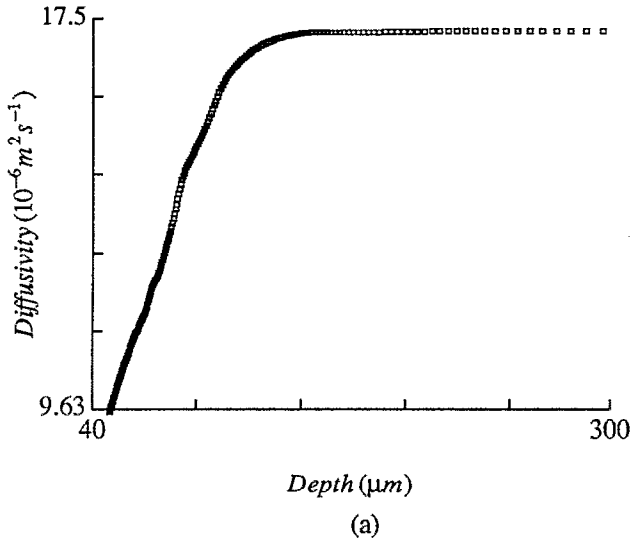

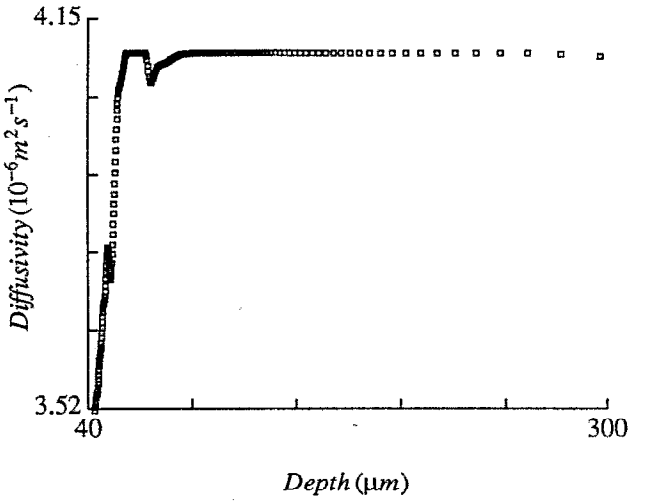

FIG. 7. Reconstructed thermal diffusivity profile of stainless-steel sample laser processed at a lower power density compared to the sample in Fig. 6(b).

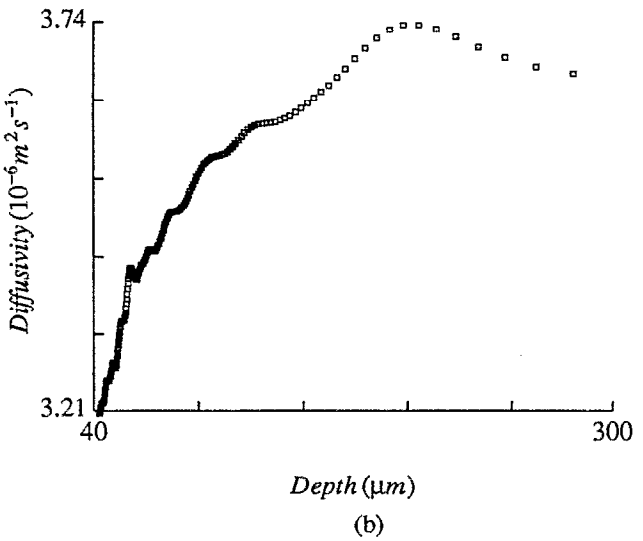

FIG. 6. Reconstructed thermal diffusivity profile of laser processed (a) low carbon steel sample and (b) stainless-steel sample from the data shown in Fig. 2.

$=4\times10^{-6}$ m^2/s, typical for stainless steel. In all three cases the first (highest frequency) solution converged in less than ten iterations and the rest in only two iterations. Figure 5 shows that the reconstructed profiles obtained from local values are in excellent agreement with the original profiles.

The algorithm described was then used to obtain thermal diffusivity profiles from the low carbon steel data shown in Figs. 2(a) and 2(c). The reconstructed profile for the laser processed low carbon steel sample is shown in Fig. 6(a). This profile shows that the thermal diffusivity starts decreasing from a depth of about 130 μm which is in agreement with the hardness profile [Fig. 4(b)]. Bulk thermal diffusivity α_∞ ($=17.3\times10^{-6}$ m^2 s^{-1}) for this sample was calculated from the thermal conductivity (k), specific heat (c), and density (ρ) values for this type of carbon steel.[11] Diffusivity has monotonically dropped to 9.7 $\times10^{-6}$ m^2 s^{-1} at a depth of 50 μm (corresponding to the highest frequency) from the surface starting from the bulk value at about 130 μm. A similar trend in thermal diffusivity decreasing with increase in hardness in carbon steel has been reported earlier.[7,12] The deepest probing depth corresponding to the lowest frequency is less than 300 μm. This is much smaller than the surface heating area (1.5 mm diameter spot) so that the heat flow is essentially one dimensional which satisfies Eq. (2).

Figure 6(b) shows the profile for the laser processed stainless-steel sample from the data shown in Figs. 2(b) and 2(d). Bulk diffusivity (α_∞) calculated from k, c, and ρ values obtained from Ref. 11 for stainless steel is 4.1 $\times10^{-6}$ m^2 s^{-1}. Thermal diffusivity starts to decrease around 200 μm from the surface which is, again, in good agreement with the hardness profile of Fig. 4(a). The rate of decrease in diffusivity is found to have changed (become steeper) at depths shallower than 55 μm which may correspond to the equiaxied crystal layer seen in the optical metallograph [Fig. 3(a)]. It should be remembered that the picture shows a variation in the depth of this layer across a surface area cross section five times smaller than the probing area of the photoacoustic detector, controlled by the laser beam spot size (1.5 mm). Therefore, the profile we obtained is an average over these variations, which, nevertheless, shows remarkable correlation with the more localized hardness profile and cross sectional photograph. The hump in the reconstructed profile of the stainless-steel sample near the lower layer boundary may be an artifact due to the sharp boundary which is a deviation from the continuous inhomogeneity. Figure 7 shows the thermal diffusivity profile of a stainless-steel sample laser processed with a lower power density where the scan speed was the same (1 in./s) but the processing laser beam spot size has

increased to 0.7 mm. This reconstruction shows a thinner damaged layer than the profile in Fig. 6(b), as expected.

One obvious problem with the steel samples is the difference in surface absorption between sample and reference. This may lead to an inaccurate PA amplitude ratio. Computer simulations have shown that when the amplitude ratio is multiplied by a small constant, the diffusivity profile shifts with respect to depth without changing the shape. Since an overall shift in the phase or the magnitude due to instrumental effects can also change the profile, it is very important to record the data from both the sample and the reference immediately after each other.

IV. DISCUSSION AND CONCLUSIONS

In this work we have established a reliable technique to obtain thermal diffusivity depth profiles of a layer extending from the surface into the bulk from the frequency domain surface data. We have also observed that the thermal wave technique as represented by photoacoustic detection is very sensitive to surface hardening due to laser processing in steels. Previous work[7,12] on steel surface hardening (achieved by increasing the carbon concentration at high temperatures) has shown that hardening reduces the thermal diffusivity of steel. The profiles obtained are in agreement with the earlier work and with observations made by destructive methods such as the optical microscope cross sectional imaging and the microhardness test, and have better resolution compared to microhardness test.

Although we have machined the samples to fit the commercially available photoacoustic cell, it is possible to design a cell so that the original specimen could be tested. Specially designed cells have been used[13,14] to examine samples of rather complex geometry by photoacoustic imaging. It may also be advantageous to use a truly nondestructive, remote detection method such as photothermal radiometry (IR emission): Although a higher power laser is required to obtain a good signal-to-noise ratio, the radiometric method has the advantage of testing samples of any size and shape, and is currently under investigation in this laboratory.

ACKNOWLEDGMENTS

Partial support of this project by the Natural Sciences and Engineering Research Council of Canada is gratefully acknowledged. One of us (T.C.M.) wishes to thank the Chinese National Commission of Education for funding his research leave, which made this work possible. We would also like to thank Professor W. W. Duley, Department of Physics, University of Waterloo for his support in preparing the laser processed samples. Technical assistance by Fred Neub in metallographic examination of samples is gratefully appreciated.

[1] R. L. Thomas, L. D. Favro, and P. K. Kuo, Can. J. Phys. **64**, 1234 (1986).
[2] M. Munidasa and A. Mandelis, in *Progress in Photoacoustic and Photothermal Sciences and Technology*, edited by A. Mandelis, Vol. 1 (Elsevier, New York, 1991), Chap. 6, p. 299.
[3] A. Mandelis, J. Math. Phys. **26**, 2676 (1985).
[4] A. Mandelis, S. B. Peralta, and J. Thoen, J. Appl. Phys. **70**, 1761 (1991).
[5] A. Mandelis, E. Schoubs, S. B. Peralta, and J. Thoen, J. Appl. Phys. **70**, 1771 (1991).
[6] W. M. Steen, in *Applied Laser Tooling*, edited by O. D. D. Soares and M. Perez-Amor (Martinus Nijhoff, 1987), p. 133.
[7] J. Jaarinen, A. Lehto, and M. Luukkala, *1983 Ultrasonic Symposium Proceedings*, edited by B. R. McAvoy (IEEE, New York, 1983), p. 659.
[8] H. J. Vidberg, J. Jaarinen, and D. O. Riska, Can. J. Phys. **64**, 1178 (1986).
[9] A. Rosencwaig and A. Gersho, J. Appl. Phys. **47**, 64 (1976).
[10] A. Ralston and P. Rabinowitz, *First Course in Numerical Analysis* (McGraw-Hill, New York, 1978), p. 392.
[11] *Metals Handbook, Desk Edition*, edited by H. E. Boyer and T. L. Gall (American Society of Metals, Metals Park, Ohio, 1985).
[12] J. Jaarinen and M. Luukkala, J. Phys. (Paris) **C6-44**, 503 (1983).
[13] L. J. Inglehart, R. L. Thomas, and J. Schuldies, J. Nondestr. Eval. **1**, 287 (1980).
[14] K. Grice, L. D. Favro, P. K. Kuo, and R. L. Thomas, in *Review of Progress in Quantitative Nondestructive Evaluation*, Vol. 2B, edited by D. O. Thompson and D. E. Chimenti (Plenum, New York, 1983), p. 1019.